



Radial polarisation patterns identify macular damage: a machine learning approach

Gary P Misson, Stephen J Anderson & Mark C M Dunne

To cite this article: Gary P Misson, Stephen J Anderson & Mark C M Dunne (07 Oct 2024): Radial polarisation patterns identify macular damage: a machine learning approach, Clinical and Experimental Optometry, DOI: [10.1080/08164622.2024.2410890](https://doi.org/10.1080/08164622.2024.2410890)

To link to this article: <https://doi.org/10.1080/08164622.2024.2410890>



© 2024 The Author(s). Published by Informa UK Limited, trading as Taylor & Francis Group.



Published online: 07 Oct 2024.



Submit your article to this journal [↗](#)





View related articles [↗](#)



View Crossmark data [↗](#)

Radial polarisation patterns identify macular damage: a machine learning approach

Gary P Misson , Stephen J Anderson  and Mark C M Dunne 

School of Optometry, Aston University, Birmingham, UK

ABSTRACT

Clinical relevance: Identifying polarisation-modulated patterns may be an effective method for both detecting and monitoring macular damage.

Background: The aim of this work is to determine the effectiveness of polarisation-modulated patterns in identifying macular damage and foveolar involvement using a methodology that involved feature selection, Naïve Bayes supervised machine learning, cross validation, and use of an interpretable nomogram.

Methods: A cross-sectional study involving 520 eyes was undertaken, encompassing both normal and abnormal cases, including those with age-related macular disease, diabetic retinopathy or epiretinal membrane. Macular damage and foveolar integrity were assessed using optical coherence tomography. Various polarisation-modulated geometrical and optotype patterns were employed, along with traditional methods for visual function measurement, to complete perceptual detection and identification measures. Other variables assessed included age, sex, eye (right, left) and ocular media (normal, pseudophakic, cataract). Redundant variables were removed using a Fast Correlation-Based Filter. The area under the receiver operating characteristic curve and Matthews correlation coefficient were calculated, following 5-fold stratified cross validation, for Naïve Bayes models describing the relationship between the selected predictors of macular damage and foveolar involvement.

Results: Only radially structured polarisation-modulated patterns and age emerged as predictors of macular damage and foveolar involvement. All other variables, including traditional logMAR measures of visual acuity, were identified as redundant. Naïve Bayes, utilising the Fast Correlation-Based Filter selected features, provided a good prediction for macular damage and foveolar involvement, with an area under the receiver operating curve exceeding 0.7. Additionally, Matthews correlation coefficient showed a medium size effect for both conditions.

Conclusions: Radially structured polarisation-modulated geometric patterns outperform polarisation-modulated optotypes and standard logMAR acuity measures in predicting macular damage, regardless of foveolar involvement.

ARTICLE HISTORY

Received 29 March 2024
Revised 22 September 2024
Accepted 24 September 2024

KEYWORDS

FCBF feature selection; machine learning; macular disease; naïve bayes; polarisation pattern perception

Introduction

Polarised light perception is a well-documented phenomenon in various animal groups, including insects, crustaceans, fish and birds.¹ This ability enhances their understanding of the environment and facilitates interactions within it, providing additional visual information to aid navigation, camouflage, predation and social communication.

Unlike many animals, humans lack dedicated retinal receptors or higher-order neurons for processing polarised light.² Despite this, humans can still perceive polarised light, although this ability has long been considered rudimentary and limited to the entoptic phenomenon known as Haidinger's brushes.³ This phenomenon appears as a faint, hourglass-shaped pattern ('brushes') near the point of fixation when viewing a uniformly polarised field, where the angle of polarisation is constant across the entire area. This effect is particularly noticeable in fields rich in blue wavelengths.

The precise basis of human polarisation perception remains unclear, but it is generally agreed that this ability is due to selective absorption of polarised light within the inner layers of the fovea before light reaches the photoreceptors.

The absorbing components are most likely oriented macular pigment molecules within radially symmetric photoreceptor cell axons.⁴ This arrangement effectively creates a diattenuating structure within the foveal retina, producing a luminance contrast signal that is perceived after subsequent neural processing.⁵

Efforts to understand human polarisation perception using uniform fields of polarised light have been hindered by the short-lived nature of Haidinger's brushes, which fade within a few seconds due to retinal adaptation. However, recent evidence shows that this perceptual ability is not limited to the use of uniform fields.⁶ Greater success in understanding polarisation vision has been achieved with regionally variable (i.e., non-uniform) polarisation fields.

Humans are remarkably sensitive to such fields, capable of detecting differences in polarisation angles of less than 5 degrees – similar to the sensitivity reported in invertebrates.⁷ This sensitivity is mainly due to the preservation of edge boundaries where there is an abrupt change in the direction of the polarised field. This edge-preserving property of non-uniform fields allows the generation of

sophisticated, temporally stable and quantifiable stimuli, including two-dimensional geometric patterns and optotypes.⁶

The dependence of polarisation perception on macular pigment and normal macular spatial ordering suggests that sensitivity measurements using polarisation targets may provide a unique means of quantifying any disruption in normal macular structure or function. The sensitivity of both Haidinger's brushes^{8,9} and polarisation-modulated spatial patterns^{10,11} to macular damage is well described. However, it is not clear which stimuli, if any, are best suited for the detection of macular damage, or the benefit of polarisation perception over more traditional methods of vision measurement (e.g., logMAR visual acuity). Furthermore, it is not clear to what extent any polarisation perception deficit is localised to the macula in general or more specifically to the foveola.

To address the challenges inherent in analysing complex and extensive datasets, a machine learning approach was implemented. The dataset included a diverse group of individuals, both with and without macular disease, who had undergone various visual assessments with polarisation-modulated patterns and conventional measures of visual acuity. By leveraging machine learning, the aim was to explore the predictive potential of these visual patterns in identifying macular disease and its specific involvement of the fovea.

Unlike traditional statistical methods that rely on pre-defined hypotheses, machine learning excels at uncovering patterns and relationships within data. This approach is particularly adept at extracting valuable insights from complex datasets, often revealing patterns that elude traditional methods. By applying machine learning to the dataset, relevant features that might not have been apparent through conventional analyses were extracted and analysed.

The machine learning strategy consisted of several key steps. First, a feature selection technique was applied to eliminate redundancy and identify the most important variables in the dataset. Next, a Naive Bayes classification algorithm was used to distinguish between individuals with and without macular disease based on the selected features. To ensure the robustness of the results, cross-validation was performed, assessing the generalisability of the model by testing it on different data subsets. Finally, nomograms were developed to facilitate interpretation of the model output in terms of log-odds ratios.

Methods

A cross-sectional study was conducted to evaluate the clinical data of both staff and adult patients at the South Warwickshire NHS Foundation Trust in the UK. This research was reviewed by independent ethical review boards and conforms with the principles and applicable guidelines for the protection of human subjects in biomedical research.

The study adhered to the tenets of the Declaration of Helsinki and was approved by the UK NHS Health Research Authority (IRAS project ID 224,715) following Research Ethics Committee approval (reference 17/WA/0180). All participants gave informed consent following explanation of the nature of the study.

Participant characteristics

Participants recruited for the study comprised individuals with both eyes healthy, one or both eyes pseudophakic but with no other pathology, and normophakic or pseudophakic individuals with age-related macular disease, diabetic retinopathy or epiretinal membrane in one or both eyes. Exclusion criteria were withdrawal of consent, inability to record a logMAR visual acuity and corneal pathology.

The ocular data sets comprised data from one eye chosen at random from the healthy/healthy pseudophakic participant group, together with data from one or both eyes of the individuals with abnormal eyes (i.e., participants with age-related macular disease, diabetic retinopathy or epiretinal membrane). The use of data from both eyes of one individual with eye pathology is justified by interocular asymmetry of pathology and/or different pathologies.^{10,11} Only participants that had a complete data set were included in the statistical analyses. In total, 520 eyes were included, of which 309 were normal, 115 had age-related macular disease (79% with foveolar involvement), 57 had diabetic retinopathy (29.8% with foveolar involvement) and 39 had epiretinal membrane (71.8% with foveolar involvement). See [Table 1](#) for further details.

Macular assessment

Diagnostic categorisation was based on history and clinical assessment, including slit-lamp biomicroscopy, dilated funduscopy and optical coherence tomography (OCT).

A Topcon DRI OCT Triton Plus swept-source OCT system, equipped with proprietary automatic image algorithms, was used for macular assessment. The OCT images were standard machine-generated outputs with no additional pre-processing. All images were of sufficient quality to support a clinical diagnosis (machine image quality index > 40). Diagnosis and disease grading were based on the evaluation of 7.0 × 7.0 mm (512 × 256 pixel) macular raster scans, with foveolar integrity assessed using horizontal and vertical 9 mm (1024 pixel) line scans through the foveola. Retinal layers were identified according to the international OCT consensus.¹²

Age-related macular degeneration was classified using the Age-Related Eye Disease Study (AREDS) system for fundus photography,¹³ which includes four levels: small drusen (7.8% of cases); small and intermediate drusen with retinal pigment epithelial changes (15.7%); small to large drusen with foveal-sparing geographic atrophy (19.1%); and foveal-involving geographic atrophy and/or evidence of choroidal neovascularization (57.4%).

Diabetic retinopathy classification was based on the Royal College of Ophthalmologists, UK, Diabetic Retinopathy Guidelines,¹⁴ which includes six grades of retinopathy: eyes with background (29.8% of cases), pre-proliferative (5.3%) and proliferative (19.3%) retinopathy in the absence of

Table 1. Participant summary data. The variables marked with an asterisk were discretised to three separate intervals using Orange data mining software (version 3.36.2). See text for details.

Variable	Number of Eyes		
Eye	255 (Left)	265 (Right)	–
Age (years)*	124 (<63)	200 (63–77)	196 (>77)
Sex	289 (Female)	231 (Male)	–
LogMAR VA*	209 (<0.11)	164 (0.11–0.32)	147 (>0.32)
Ocular Media	281 (Normal)	145 (Pseudophakic)	94 (Cataract)

maculopathy; and eyes with background (33.3%), pre-proliferative (10.5%) and proliferative (1.8%) retinopathy in the presence of maculopathy.

Epiretinal membrane was classified using the grading scheme of Govetto et al.¹⁵ which includes four stages: presence of foveal pit with well-defined retinal layers (30.8% of cases); absence of pit with well-defined layers (33.3%); absence of pit with well-defined layers and presence of ectopic inner foveal layers (20.5%); and absence of pit with disrupted retinal layers and presence of ectopic inner foveal layers (15.4%).

In addition to these published methods of disease classification, a further disease classification based on OCT-defined foveolar structural changes was employed because polarisation sensitivity is confined to this region of the retina.⁷ The outer boundary of the foveola was defined on OCT as the termination of the inner nuclear layer (Figure 1). Foveolar involvement in abnormal eyes was defined as any OCT-identifiable structural abnormality at any level of the retina confined by the boundary of the termination of the inner nuclear layer.

Clinical interpretation and grading were conducted by the first author (GPM), an experienced practising consultant ophthalmologist. Grading was completed without prior knowledge of the psychophysical results. Decisions were not reviewed by other ophthalmologists.

Data acquisition and polarization pattern perception

Conventional, corrected distance logMAR visual acuity (VA) was measured using a standard Bailey-Lovie chart.

The method of polarisation pattern perception measurement is detailed elsewhere.^{10,11} Briefly, participants were asked to identify images presented using a polarisation stimulus generator consisting of a modified liquid crystal display (Asus VS278H from ASUSTeK Computer Inc., Taiwan).^{6,7,16}

Standard polarimetry and photometric methods⁷ confirmed that the polarisation output was dependent on shades of screen grey and predominantly linearly polarised (degree of linear polarisation ≥ 0.94). The angles of polarisation varied from 54° for the darkest grey (foreground of stimulus images) to 147° for the lightest grey (background of stimulus images). The display screen, viewed from 3 m, subtended a visual angle of 11° (width) \times 6.5° (height) and emitted blue light with a peak wavelength of 460 nm at a consistent luminance of 8.0 cd/m^2 for all grey-scale values.

The stimulus set comprised 14 geometric patterns, to include patterns that accord with the radial architecture of the macula, and both logMAR-graded and contrast-graded Sloan optotypes, as detailed below. Figure 2 shows examples of the polarisation-modulated patterns employed in this study, together with their simulated foveal fixation percepts.

Three pattern response criteria were used: (i) identification, defined as the ability to identify accurately the stimulus pattern/optotype; (ii) detection, defined as the ability to detect but not identify the presence of a pattern, and (iii) not detected. Previous investigations by the present authors have established that individual responses for the criteria of 'identified', 'detected' and 'not detected' give repeatable, clinically useful results.^{10,11}

Stimulus patterns were displayed in a pseudorandom order, with the presentation managed by one of two trained ophthalmic technicians, neither of whom knew the diagnoses of participants. All testing was done monocularly, with each eye of a participant assessed in turn. Participants were informed that a series of images would be shown one at a time, and they would have a maximum of 30 seconds to view each image. They were instructed to focus on the centre of the display screen for each image presentation.

Although the possibility of eccentric fixation was not monitored, the advantage of this protocol is that polarisation perception requires fixation at the fovea, as this phenomenon only occurs there. All participants were able to perceive at least some polarisation targets, confirming fixation.

For each image, participants were asked whether they saw a pattern or just a blank blue screen. A positive response was recorded as pattern detection. Those who detected a pattern were then asked to describe it. A positive response for pattern identification was recorded if the participant could describe the general appearance of the displayed image. Accepted description terms included vertical stripes or bars, concentric circles or rings, checks or chequerboard, star or starburst, and windmill or triangles. Letter identification was required for optotype images. The typical duration for viewing the full series of images was between 10 and 15 minutes per eye.

All measurements were taken with normal, undilated pupils. Ametropic participants were corrected for the display screen working distance using isotropic trial lenses (i.e., lenses that do not alter the state of polarisation of

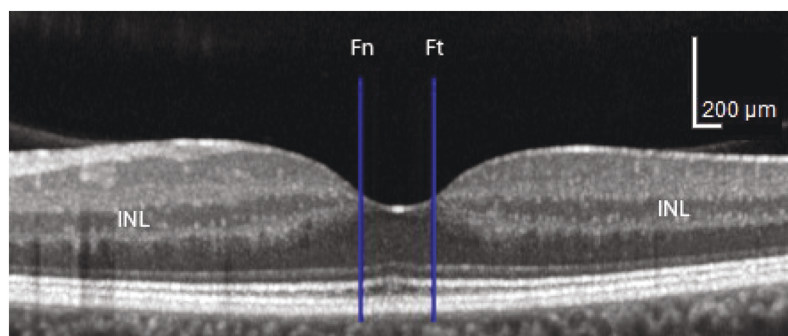


Figure 1. Horizontal OCT scan through the foveolar centre of a healthy macula (left eye). The boundary of the foveola is defined by the termination of the inner nuclear layer (INL), indicated by the blue line nasally at Fn and temporally at Ft.

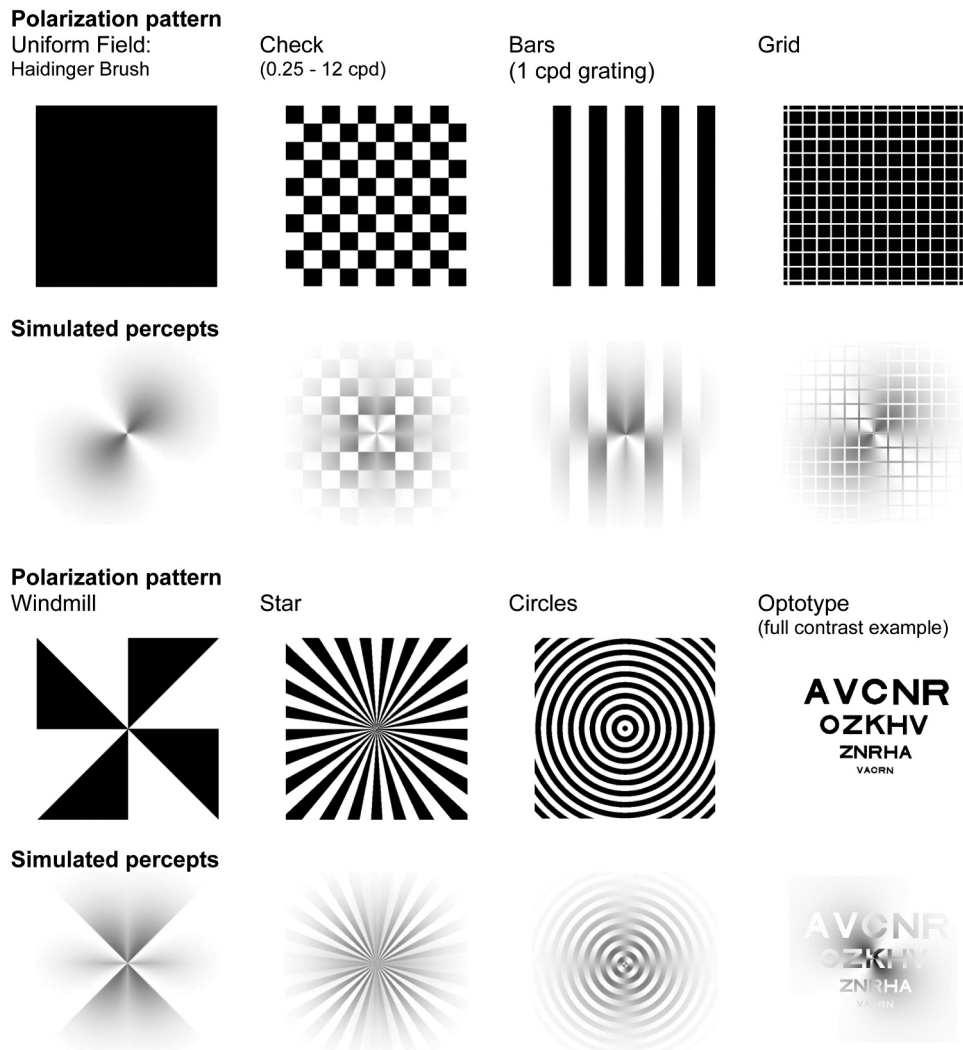


Figure 2. Representation of the polarisation-modulated geometric and optotype patterns used, together with their simulated foveal fixation percepts. Static chequerboard patterns varied in check size, with their fundamental spatial frequency spanning the range of frequencies over which polarisation patterns are visible.⁷ A dynamic chequerboard with a fundamental frequency of 1 cpd alternating at 1 hz was included as it is routinely employed in clinical visual measures. A uniform field alternating at 1 hz was used to generate a dynamic Haidinger's brush; a non-alternating field was used to generate a static Haidinger's brush. The optotype examples shown here are high contrast logMAR graded as used in the calculation of polar logMAR. Reduced polarisation contrasts for logMAR 1.0 optotypes (not shown) were used for polar contrast scores (see text for explanation).

light transmitted through them). The lenses were supported in a trial frame.

Data quantification and statistical methods

Orange (version 3.36.2), an open-source data mining software for machine learning applications, was used for all analyses. The organisation of graphical elements, called widgets, in the developed Orange data processing workflow is shown in Figure 3.

The machine learning approach involved feature selection followed by Naïve Bayes supervised machine learning. To complete the analyses, it was necessary to discretise the continuous data (age and acuity measures) into separate intervals. This was done using the 'Discretise' widget of the Orange data mining software.

The number of features (independent variables) selected is critical to subsequent machine learning performance. In this study, 21 features were investigated, including eye (right, left), age in years (<63, 63–77, >77), sex (male, female), ocular media (normal, pseudophakic, cataract), conventional logMAR visual acuity, 14 perceptual measures of

polarisation-modulated geometric patterns (identified, seen, not seen), and two evaluations (scores) based on the identification of polarisation-modulated logMAR-graded Sloan optotypes (termed Polar logMAR) and contrast-graded Sloan optotypes (termed Polar Contrast).

Polar logMAR was calculated as the total number of high-contrast optotypes identified from a set of 50 (displayed in five-letter groups) that ranged in size from 1.2 logMAR to 0.2 logMAR. Polar Contrast was calculated as the total number of 1.0 logMAR sized optotypes identified from a set of 24 (displayed in three-letter groups) that varied in polarisation-equivalent contrast (defined in Misson and Anderson⁷) from 0.75 to 0.05.

Two targets (dependent variables) were investigated: macular damage and foveolar involvement (both with binary classification of 'no' or 'yes'). In preliminary analyses, an attempt was made to target the disease classifications of age-related macular disease, diabetic retinopathy and epiretinal membrane. However, the number of cases for specific disease classifications was too low, as shown by confusion matrices constructed from the results of Naïve Bayes machine learning, which failed to detect any epiretinal membrane

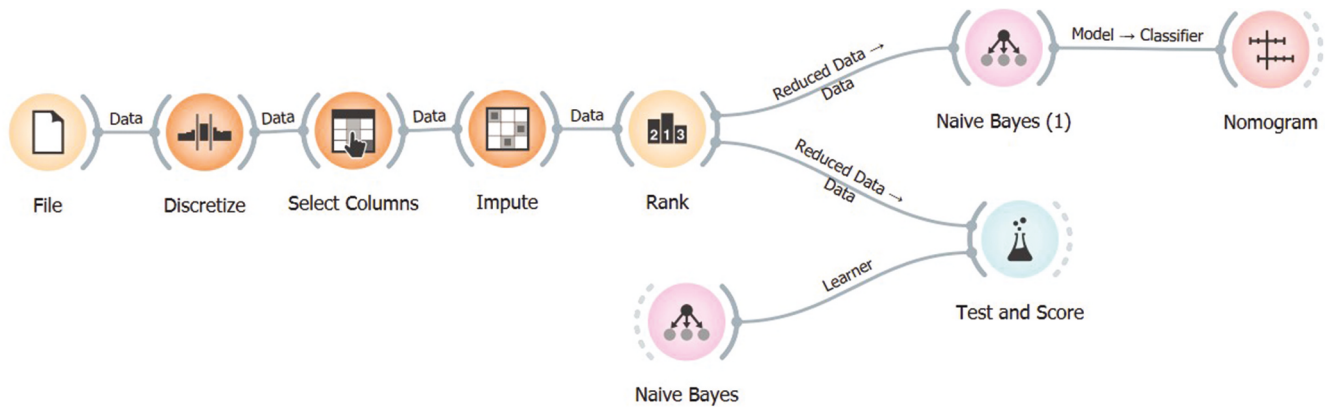


Figure 3. Orange workflow for the Fast Correlation-Based Filter (FCBF) feature ranking and Naïve Bayes supervised machine learning. 'File' reads the data input (from an Excel spreadsheet). 'Discretize' converted numeric variables into three interval categories (age <63, 63–77, >77 years; logMAR VA < 0.11, 0.11–0.32, >0.32; polar logMAR < 0.5, 0.5–4.5, >4.5; polar contrast <0.5, 0.5–2.5, >2.5). 'Select columns' allowed manual assignment of features (21 independent variables: eye, age, sex, ocular media, logMAR VA, 14 perceptual measures of polarisation-modulated geometric patterns, polar logMAR and polar contrast) and targets (two dependent variables: macular damage and foveolar involvement, both with binary classification of 'no' or 'yes'). The 'impute' widget removed participants with incomplete data sets. 'Rank' used the FCBF feature selection method^{17,18} to remove redundant features for each target. 'Naïve Bayes' provided the supervised machine learning classification model. The same model was placed in two positions to explore its performance ('Naïve Bayes') and log-odds ratios ('Naïve Bayes (1)'). 'Test and score' provided performance measures of Naïve Bayes – both Matthews Correlation Coefficient (MCC) and the area under the receiver operating characteristic curve (AUC) were determined after stratified 5-fold cross validation. 'Nomogram' showed the log-odds ratios from the Naïve Bayes models (i.e., log likelihood ratios) for the targets macular damage and foveolar involvement.

cases (Matthews correlation coefficient < 0.001) and detected only one diabetic retinopathy case (Matthews correlation coefficient = 0.021).

The Fast Correlation-Based Filter (FCBF) feature selection method^{17,18} was employed. This method efficiently removes redundant features (independent variables) so that those selected are highly correlated to the specified target (dependent variable) but not correlated to each other. It works by evaluating the relevance of each feature to the target using Symmetrical Uncertainty, an entropy-based measure that quantifies the shared information between two variables.

Features with symmetrical uncertainty values above a threshold, determined from the data distribution to avoid user bias, are considered relevant and ranked accordingly. The algorithm then iteratively removes redundant features by comparing their uncertainty values with those of already selected features, ensuring that only unique and informative features are retained. By focusing on both relevance and redundancy, the FCBF method ensures that the selected features are both informative and non-redundant. It has become one of the most common feature selection methods in use.¹⁸

The same 21 features (i.e., independent variables identified above) were presented to the FCBF selection method to determine which were important for detecting macular damage or foveolar involvement.

To provide more information about the influence of selected features on the specified targets, and to estimate the size effect, Naïve Bayes supervised machine learning was employed. Naïve Bayes is the simplest form of machine learning algorithm and there were three main reasons for choosing this model. First, unlike other machine learning algorithms, Naïve Bayes does not require hyperparameter tuning (i.e., adjusting model settings to achieve the best possible performance). Second, Orange Data Mining software conveniently connects Naïve Bayes to its nomogram widget, which reveals the Log-odds ratios involved in making predictions. Thirdly, although the FCBF method largely mitigates concerns about violating the conditional independence

assumption of Naïve Bayes, the algorithm is known to perform well even when the independence assumption is not valid.^{19–21}

The data split for training and testing was carried out automatically via the Orange 'Test and Score' widget using a 5-fold cross validation process, a well-known machine learning technique that provides a reliable estimation of model performance.^{22,23} With this technique, the sample is randomly divided into five separate groups (or folds), each stratified to maintain approximately equal proportions of the outcome variable. During the first run, the first fold is held out for testing while the other four folds are used to train the prediction model.

In the second run, the second fold is held out for testing and the remaining four folds are used for training. This process continues until each of the five folds has been used for both training and testing, resulting in five separate testing groups. This approach prevents overfitting that would occur if the prediction model were tested on the same data used for training.

Collins et al.²⁴ summarise the latest recommendations for evaluating prediction models, referring to the TRIPOD statement (Transparent Reporting of a multivariable prediction model for Individual Prognosis Or Diagnosis). The approach used in this study aligns with their analysis type B: 'Model developed using all available data and its performance evaluated using resampling, such as bootstrapping or k-fold cross-validation (internal validation)'.

Estimation of the size effect involved determining Matthews correlation coefficient (MCC) for the Naïve Bayes models that were trained to predict macular damage and foveolar involvement. Matthews correlation coefficient is particularly useful for the binary classifications carried out in this study.²⁵ It approximates Pearson's correlation coefficient for the classification of supervised machine learning methods,²⁶ thereby providing an estimate of effect size in which values of 0.1, 0.3 and 0.5 represent, respectively, small, medium and large effects.²⁷

The area under the receiver operating characteristic curve (AUC), commonly used in machine learning,²² was also

determined for each model. An area under the receiver operating characteristic curve below 0.7 is suboptimal, 0.7 to 0.8 is good and above 0.8 is excellent.²⁸

Results

Table 2 shows the ranked influence of each independent variable in predicting macular damage and foveolar involvement following the FCBF feature selection method.

The 'Star' polarisation-modulated stimulus and age were selected as predictors of macular damage. All other variables, including conventional logMAR measures of visual acuity, were identified as redundant or irrelevant features. Although not selected, it is noteworthy that the third highest ranked variable was another radially structured polarisation-modulated geometric pattern, named 'Windmill'. Both the Star and Windmill geometric patterns, together with their simulated foveal fixation percepts, are shown in Figure 2.

The Windmill polarisation-modulated geometric pattern and age were selected as predictors of foveolar involvement, with all remaining features identified as redundant. It is noteworthy that the Star polarisation pattern was not selected but was nonetheless the third highest ranked variable. Of further note is that, for both macular damage and foveolar involvement, the lowest FCBF ranked variable was Eye (i.e., right or left eye of participant), which provides further support for the use of data from both eyes of each individual (see Methods).

These results are supported by standard chi-square analyses, which were used to assess the significance of the relationship between all features and the target variables. Macular damage showed significant ($p < 0.001$) associations with 16 features, with the Star pattern ranked highest based on the Chi-square value ($X^2 = 37.33$). Foveolar involvement

showed significant ($p < 0.001$) associations with 15 features, with the Windmill pattern ranked highest ($X^2 = 37.85$).

Naïve Bayes, with the FCBF selected features, provided a good prediction for macular damage (area under the receiver operating characteristic curve = 0.773), with a medium size effect (Matthews correlation coefficient = 0.458). The model also provided a good prediction for foveolar involvement (area under the receiver operating characteristic curve = 0.763), again with a medium size effect (Matthews correlation coefficient = 0.356).

The log-odds ratios (i.e., Log Likelihood ratios) for macular damage and foveolar involvement were computed to aid interpretation of Naïve Bayes predictions, allowing for more information on the relative influences of age and the selected polarisation-modulated geometrical patterns. The results are shown in Table 3. To aid clarity, the log-odds ratios for predicting macular damage and/or foveolar involvement were converted to probabilities (relative to chance, 50%). For example, failure to detect the Star polarisation-modulated pattern raises the probability of macular damage by 20.1%, whereas successfully identifying the pattern reduces it by 26.1%.

Discussion

The belief that sensitivity measures of polarisation-modulated stimuli could offer a unique method for predicting macular damage arises from the fact that humans perceive polarised light solely because diattenuating macular structures convert it into a luminance signal. This mechanism guarantees that the resulting luminance signal covers the entire extent of the fovea but does not extend beyond the macula, making it a stimulus purely targeting the macula. However, despite the use of a wide array of polarisation patterns to evaluate macular function, including uniform and non-uniform polarisation fields, polarisation-modulated optotypes and structured light, their predictive accuracy remains unclear.

In this study, a machine learning approach was utilised to assess the predictive potential of polarisation patterns for macular damage and foveolar involvement. This involved extracting relevant features from a large dataset comprising sensitivity measures and patient variables to uncover subtle trends that might otherwise be challenging to identify. Through this method, it was discovered that: (i) polarisation measures outperform conventional logMAR acuity measures in predicting macular and foveal damage; (ii) geometric patterns are more effective than polarisation-modulated

Table 2. Fast Correlation-Based Filter (FCBF) ranking of 21 independent variables (features) for predicting macular damage and foveolar involvement, with ranked order based on symmetrical uncertainty, an entropy-based correlation measure. FCBF ranking based on data from a total of 520 eyes. Features selected for inclusion in the machine learning model are bolded and marked with a double asterisk (**). Representations of the polarisation-modulated patterns are given in Figure 2. Abbreviations used: Haidinger's brushes (HB); alternating chequerboard (AltCheck); visual acuity (VA); fundamental spatial frequency in cycles/degree (# cpd); vertical square wave grating (bars). See text for definition of polar logMAR and polar contrast.

Rank	Macular Damage	Foveolar Involvement
1	Star**	Windmill**
2	Age**	Age**
3	Windmill	Star
4	Check 0.25 cpd	Check 0.25 cpd
5	Circles	Dynamic HB
6	Dynamic HB	Circles
7	Check 2 cpd	Check 2 cpd
8	AltCheck 1 cpd	Polar logMAR
9	Polar logMAR	AltCheck 1cpd
10	Bars 1 cpd	logMAR VA
11	logMAR VA	Bars 1cpd
12	Check 4 cpd	Check 6 cpd
13	Static HB	Media
14	Media	Static HB
15	Grid	Grid
16	Check 6 cpd	Check 4 cpd
17	Polar Contrast	Polar Contrast
18	Check 12 cpd	Check 12 cpd
19	Check 9 cpd	Check 9 cpd
20	Sex	Sex
21	Eye	Eye

Table 3. Log-odds ratios for predicting macular damage (top panels) and foveolar involvement (bottom panels). The Fast Correlation-Based Filter (FCBF) selected variables for predicting macular damage were the star polarisation-modulated pattern and age. The variables for predicting foveolar involvement were the Windmill polarisation pattern and age. Log-odds ratios (provided by Orange, version 3.36.2) were converted to odds values using $odds = e^{(\log \text{ odds})}$, with probability (P) determined using $p = odds/(1+odds)$. For each condition, the probability (%) for predicting pathology is expressed (in brackets) relative to chance (i.e., 50%).

Macular Damage			
	Identified	Detected	Not Detected
Star	-1.16 (-26.1%)	-0.20 (-5.0%)	0.85 (20.1%)
Age	<63 years	63-77 years	>77 years
	-1.71 (-34.7%)	0.14 (3.5%)	0.58 (14.1%)
Foveolar Involvement			
	Identified	Detected	Not Detected
Windmill	-1.37 (-29.7%)	-0.35 (-8.7%)	0.70 (16.8%)
Age	<63 years	63-77 years	>77 years
	-2.03 (-38.4%)	0.13 (3.2%)	0.58 (14.1%)

optotypes for evaluating macular function; and (iii) radially structured polarisation-modulated patterns are particularly effective for predicting both macular damage and foveolar involvement.

The present findings are based on a sample in which the majority of participants had moderate to severe retinal damage. It remains an open question as to how a more even distribution of cases from mild to severe retinal damage might have influenced the outcomes.

The FCBF feature selection method was crucial in the machine learning approach employed, which evaluated 21 independent variables. Commonly used in machine learning studies,^{17,18,29} this method effectively eliminates redundant variables, ensuring that the selected variables are highly correlated with the target (macular damage or foveolar involvement) but not with each other. This process, known as data reduction, enhances machine learning performance by highlighting the most influential predictors of macular damage.

In this study, the FCBF method identified two polarisation-modulated patterns (Star and Windmill) and age as key predictors of macular and foveolar damage. Notably, it did not select sensitivity measures related to conventional logMAR visual acuity. However, this should not be taken to suggest that visual acuity lacks predictive value or that it is unrelated to other variables, such as sex, eye or ocular media (e.g., cataracts). It is well-established, for example, that visual acuity is affected by macular disease and can also be influenced by conditions like cataracts. The FCBF method simply shows that, in this context, the predictive power of visual acuity is weaker compared to that of polarisation-modulated patterns.

Considering that macular damage is predominantly associated with ageing, the inclusion of age in the machine learning model would be expected. That it was included reinforces confidence in the FCBF feature selection method.

For readers more familiar with traditional statistics than machine learning, Chi-square analyses were conducted to examine the relationship between all features and the target variables in this study. This conventional statistical method supported the main findings: the Star pattern showed the strongest association with macular damage, while the Windmill pattern was most strongly linked to foveolar involvement (see the FCBF ranking in Table 2 for comparison).

Although the Chi-square test effectively provided traditional statistical support for the machine learning findings, it has significant limitations when used for feature selection. Specifically, the Chi-square test examines the relationship between each feature and the target variable independently, without accounting for potential redundancy among features. This limitation likely explains why significant associations were evident for most independent variables (see Results). In contrast, FCBF provides a more sophisticated approach by directly addressing feature redundancy.

As noted above, FCBF efficiently identifies a minimal subset of features that are strongly correlated with the target variable while minimising redundancies among them. In other words, the few selected features collectively provide all the necessary information for identifying the target. As a result, FCBF yielded a more robust and informative feature set for subsequent modelling using Naïve Bayes.

Both selected polarisation-modulated patterns, specifically the Star and Windmill patterns, feature radial geometric

structures. The Star pattern ranked highest among the FCBF features for predicting macular damage, while the Windmill pattern ranked highest for predicting foveolar involvement. These patterns were designed based on the radial dispersion of the Henle fibre layer from the foveal centre in a healthy macula. It is hypothesised that the shared radial symmetry between the architecture of the retina and the polarisation pattern confers an advantage over visual patterns lacking radial symmetry. In brief, disruptions in the radial structure of the macula through disease may be most effectively identified using a corresponding radially structure stimulus.

The reasons behind the differing rankings of the Star and Windmill patterns for predicting macular damage are unclear. The sole distinction between these two polarisation patterns lies in their angular frequency: the Star pattern features an angular frequency of $\pi/12$, while the Windmill pattern has an angular frequency of $\pi/2$ (Figure 2). Considering that a shared radial symmetry between the visual stimulus and macular architecture offers the most advantageous scenario for assessing macular function, a speculation is that the greater density of radial pattern features at higher eccentricities for the Star pattern compared to the Windmill pattern may provide the former with an advantage in predicting macular damage.

Recent work by Kapahi et al.³⁰ lends support to the notion that radial patterns could be the most effective for evaluating macular function. Using structured light, they found that the visual angle over which radially patterned entoptic phenomena are perceivable is significantly larger compared with previously observed ranges for non-radial polarisation-modulated patterns.

Naïve Bayes machine learning, utilising variables selected by the FCBF method, offered a reliable prediction for macular damage and foveolar involvement, showing a medium effect size. This emphasises the clinical applicability of the findings. Not recognising the Star geometric pattern raises the probability of macular damage with intact foveal function. Not recognising the Windmill pattern raises the probability of macular damage which includes damage to the foveola. Additionally, advancing age further heightens the probability of both.

Log-odds ratios, increasingly pivotal in clinical decision-making,^{31,32} offer a straightforward interpretation of the findings. Positive and negative values indicate the extent to which suspicion should shift towards or away from a macular defect, respectively (see Table 3). Expressing these ratios as probabilities, it was observed that among individuals aged 63–77 years who cannot detect the Star pattern, there is a 46.4% higher likelihood of macular damage compared to those who can identify the pattern. Similarly, among individuals in the same age group who cannot detect the Windmill pattern, there is a 47.2% higher likelihood of macular damage with foveolar involvement compared to those who can identify the pattern.

In conclusion, radially structured polarisation-modulated geometric patterns have potential to predict both macular damage with and without foveolar involvement, surpassing various other polarisation patterns, including optotypes, and standard logMAR measures of visual acuity. The observed medium-size effects support the need for further investigation into developing a clinical nomogram for predicting macular damage, as artificial intelligence-based models hold significant promise for integration into clinical ophthalmic practice.

Acknowledgements

The authors thank David Reynolds and Mark Gillett for their technical support. GPM received a grant from the European Society of Cataract and Refractive Surgeons for this work.

Disclosure statement

No potential conflict of interest was reported by the author(s).

Funding

The work was supported by the European Society of Cataract and Refractive Surgeons.

ORCID

Gary P Misson  <http://orcid.org/0000-0001-8843-8389>

Stephen J Anderson  <http://orcid.org/0000-0002-5719-2846>

Mark C M Dunne  <http://orcid.org/0000-0001-9126-0702>

References

- Cronin TW, Shashar N, Caldwell RL et al. Polarization vision and its role in biological signaling. *Integr Comp Biol* 2003; 43: 549–558.
- Land MF, Nilsson DE. *Animal eyes*. Oxford, UK: Oxford University Press; 2002.
- Haidinger H. *Annalen der Physik und Chemie*. JC Poggendorf, editor. Vol. 63. Berlin, Germany; 1844. p. 29.
- McGregor J, Temple SE, Horváth G. Human polarization sensitivity. In: Horváth G, editor. *Polarized light and polarization vision in animal sciences*. 2nd ed. Heidelberg: Springer; 2014. p. 303–318.
- Misson GP, Temple SE, Anderson SJ. Polarization perception in humans: on the origin of and relationship between Maxwell's spot and Haidinger's brushes. *Sci Rep* 2020; 10: 108. doi:10.1038/s41598-019-56916-8
- Misson GP, Timmerman BH, Bryanston-Cross PJ. Human perception of visual stimuli modulated by direction of linear polarization. *Vision Res* 2015; 115: 48–57.
- Misson GP, Anderson SJ. The spectral, spatial and contrast sensitivity of human polarization pattern perception. *Sci Rep* 2017; 7: 16571. doi:10.1038/s41598-017-16873-6
- Goldschmidt M. A new test for function of the macula lutea. *Arch Ophthalmol* 1950; 44: 129–135.
- Stanworth A, Naylor EJ. The measurement and clinical significance of the Haidinger effect. *Trans Ophthalmol Soc UK* 1955; 75: 67–79.
- Misson GP, Anderson SJ, Armstrong RA et al. The clinical application of polarization pattern perception. *Trans Vis Sci Tech* 2020; 9: 31.
- Misson GP, Anderson SJ, Armstrong RA et al. The effect of age-related macular degeneration on polarization pattern perception. *Trans Vis Sci Tech* 2021; 10: 8.
- Staurenghi G, Sadda S, Chakravarthy U et al. Proposed lexicon for anatomic landmarks in normal posterior segment spectral-domain optical coherence tomography: the INOCT consensus. *Ophthalmol* 2014; 121: 1572–1578.
- Age-Related Eye Disease Study Research Group. The age-related eye disease study system for classifying age-related macular degeneration from stereoscopic color fundus photographs: the age-related eye disease study report. *Am J Ophthalmol* 2001; 132: 668–681.
- Royal College of Ophthalmologists UK. *Diabetic retinopathy guidelines*. London, UK: Royal College of Ophthalmologists; 2012.
- Govetto A, Lalane RA, Sarraf D et al. Insights into epiretinal membranes: presence of ectopic inner foveal layers and a new optical coherence tomography staging scheme. *Am J Ophthalmol* 2017; 175: 99–113.
- Temple SE, McGregor JE, Miles C et al. Perceiving polarization with the naked eye: characterization of human polarization sensitivity. *Proc R Soc B* 2015; 282: 20150338.
- Yu L, Liu H. Feature selection for high-dimensional data: a fast correlation-based filter solution. *Proceedings of the 20th international conference on machine learning (ICML-2003)*; 2003; Washington DC.
- Naser MA, Majeed AA, Alsabah M et al. A review of machine learning's role in cardiovascular disease prediction: recent advances and future challenges. *Algorithms* 2024; 17: 78. doi:10.3390/a17020078
- Domingos P, Pazzani M. On the optimality of the simple bayesian classifier under zero-one loss. *Mach Learn* 1997; 29: 103–130.
- Zhang H. The optimality of naive Bayes. *Proceedings of the 17th international Florida artificial intelligence research society conference, American Association for Artificial Intelligence, Florida, USA*; 2004.
- Cosma G, Brown D, Archer M et al. A survey on computational intelligence approaches for predictive modeling in prostate cancer. *Exp Syst Appl* 2017; 70: 1–19.
- Lu W, Tong Y, Yu Y et al. Applications of artificial intelligence in ophthalmology: general overview. *J Ophthalmol* 2018; 2018: 1–15.
- Demšar J, Zupan B, Palagi PM. Hands-on training about overfitting. *PLOS Comput Biol* 2021; 17: e1008671. doi:10.1371/journal.pcbi.1008671
- Collins GS, Dhiman P, Ma J et al. Evaluation of clinical prediction models (part 1): from development to external validation. *BMJ* 2024; 384: e074819. doi:10.1136/bmj-2023-074819
- Chicco D, Jurman G. The advantages of the Matthews correlation coefficient (MCC) over F1 score and accuracy in binary classification evaluation. *BMC Genomics* 2020; 21: 6. doi:10.1186/s12864-019-6413-7
- Powers DM. Evaluation: from precision, recall and F-measure to ROC, informedness, markedness and correlation. *ArXiv, abs/2010.16061* 2011.
- Prajapati B, Dunne M, Armstrong R. Sample size estimation and statistical power analyses. *Optometry Today*. 2010; 16: 10–18.
- D'Agostino RB, Pencina MJ, Massaro JM et al. Cardiovascular disease risk assessment: insiGlob Heartts from framingham. *Glob Heart* 2013; 8: 11–23.
- Jaber AA. Diagnosis of bearing faults using temporal vibration signals: a comparative study of machine learning models with feature selection techniques. *J Fail Anal Preven* 2024; 24: 752–768.
- Kapahi C, Silva AE, Cory DG et al. Measuring the visual angle of polarization-related entoptic phenomena using structured light. *Biomed Opt Express* 2024; 15: 1278–1287.
- Tan TE, Xu X, Wang Z et al. Interpretation of artificial intelligence studies for the ophthalmologist. *Curr Opin Ophthalmol* 2020; 31: 351–356.
- Hasan MM, Phu J, Sowmya A et al. Artificial intelligence in the diagnosis of glaucoma and neurodegenerative diseases. *Clin Exp Optom* 2024; 107: 130–146.